An "adiabatic-hindered-rotor" treatment allows *para*-H_2 to be treated as if it were spherical

Hui Li,[1,2] Pierre-Nicholas Roy,[2] and Robert J. Le Roy[2,a)]
[1]*Institute of Theoretical Chemistry, State Key Laboratory of Theoretical and Computational Chemistry, Jilin University, 2519 Jiefang Road, Changchun 130023, People's Republic of China*
[2]*Department of Chemistry, University of Waterloo, Waterloo, Ontario N2L 3G1, Canada*

(Received 25 May 2010; accepted 18 July 2010; published online 13 September 2010)

In *para*-H_2–{molecule} interactions, the common assumption that *para*-H_2 may be treated as a spherical particle is often substantially in error. For example, quantum mechanical eigenvalues on a full four-dimensional (4D) potential energy surface for *para* H_2–{linear molecule} species often differ substantially from those calculated from the corresponding two-dimensional (2D) surface obtained by performing a simple spherical average over the relative orientations of the H_2 moiety. However, use of an "adiabatic-hindered-rotor" approximation can yield an effective 2D surface whose spectroscopic properties are an order of magnitude closer to those yielded by a full 4D treatment. © *2010 American Institute of Physics*. [doi:10.1063/1.3476465]

I. INTRODUCTION

The wave function of an isolated ground-state ($J=0$) *para*-H_2 molecule is precisely spherically symmetric, and because the energy of its first excited level is relatively large (45 meV, corresponding to a collision energy of 520 K), it is often considered a good approximation to treat *para*-H_2 as a spherical particle.[1–5] This is a very attractive approximation, as it greatly reduces the computational effort associated with dynamical simulations for systems containing multiple *para*-H_2 molecules. One system for which this assumption has been critically examined is *para*-H_2–OCS.[6] In that case it was shown that calculations using a two-dimensional (2D) potential energy surface (PES) obtained simply by averaging a four-dimensional (4D) PES over all possible orientations of the H_2 monomer yielded eigenvalues which differed from those obtained from a full 4D calculation by up to 1 cm^{-1}. Nonetheless, since the discrepancies in level energy *differences* were much smaller than this, that 2D potential was used as the basis for extensive simulations of vibrational frequency shifts of OCS in clusters of 1–17 *para*-H_2 molecules.[3]

The present work examines the reliability of this spherical-averaging approximation for the three systems: *para*-H_2–CO_2, *para*-H_2–CO, and (*para*-H_2)$_2$. It shows that use of an "adiabatic-hindered-rotor" separation of the fast rotational motion of H_2 from the other degrees of freedom yields effective spherical descriptions of *para*-H_2 in *para*-H_2-{linear molecule} interactions, which are an order of magnitude more accurate than those obtained using a simple-spherical-average approximation. The same comparisons are also made for systems formed by *ortho*-D_2 with CO_2, with CO, and with itself.

In the early days of quantitative {atom}-{diatom} Van der Waals spectroscopy, some 4 decades ago, calculating bound-state level energies to experimental accuracy was a very challenging problem. For the special case of H_2-{rare gas} bimers, a relatively simple basis-set method requiring only one (carefully chosen) radial basis function sufficed,[7] but for more strongly anisotropic interactions, very tedious (at the time) coupled-equation calculations were required. In this context, the "Born–Oppenheimer angular/radial separation" approximation introduced by Holmgren *et al.*[8] was proven very useful. Although it only yielded upper- and lower-bound energies which differed (for {rare gas}-H*X* complexes, with X=F, Cl, or Br) by several cm^{-1}, it provided accurate estimates of angular and radial expectation values, and hence proved very useful in the modeling of experimental spectra in terms of realistic potential energy surfaces. More recently, Alexander and co-workers[9] reintroduced this approach under the acronym of the "adiabatic bender" (AB) approximation, and applied it to a number of open shell systems.[9–11] The present work shows that a very straightforward version of this approach, which we call the adiabatic-hindered-rotor approximation, can yield very accurate reduced-dimension descriptions of *para*-H_2-{molecule} interactions whose use greatly reduces the computational cost of simulations of *para*-H_2 cluster phenomena.

II. HAMILTONIAN AND REDUCED-DIMENSION TREATMENT

While the same considerations apply to any *para*-H_2-{molecule} or *ortho*-D_2-{molecule} system, to simplify the presentation, this section explicitly considers the interaction of a rigid *para*-H_2 molecule with a rigid, linear CO_2 molecule. As seen in Fig. 1, the geometry of this system can be described naturally using Jacobi coordinates $(R, \theta_1, \theta_2, \phi)$, where $\vec{R}$ is a vector pointing from the center of mass of CO_2 to the center of mass of H_2, θ_1 is the angle between $\vec{R}$ and a vector pointing along the CO_2 axis, θ_2 is the angle between $\vec{R}$ and a vector pointing from one H atom to the other, and ϕ is the dihedral angle between the two planes defined by $\vec{R}$ with the CO_2 molecule and with the H_2 mol-

a)Electronic mail: leroy@uwaterloo.ca.

 © 2010 American Institute of Physics

Downloaded 23 Sep 2010 to 129.97.80.64. Redistribution subject to AIP license or copyright; see http://jcp.aip.org/about/rights_and_permissions

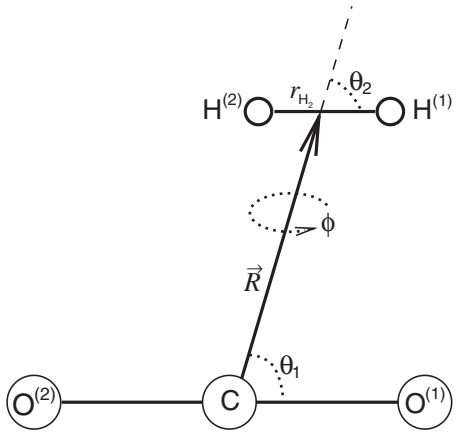

FIG. 1. Jacobi coordinates for the CO_2–H_2 system.

ecule. Within the electronic Born–Oppenheimer approximation, the four-dimensional intermolecular rovibrational Hamiltonian for this system in the space-fixed frame with CO_2 in vibrational state $(v_1,v_2,v_3)=(0,0,v_3)$ has the following form:[12–14]

$$\hat{H}_{\rm tot} = -\frac{\hbar^2}{2\mu}\frac{\partial^2}{\partial R^2} + B_{\rm CO_2}\hat{j}_1^2 + \frac{(\hat{J}-\hat{j}_1-\hat{j}_2)^2}{2\mu R^2} + \hat{H}_{\rm H_2}(\theta_2,\phi;R,\theta_1), \quad (1)$$

with

$$\hat{H}_{\rm H_2}(\theta_2,\phi;R,\theta_1) = B_{\rm H_2}\hat{j}_2^2(\theta_2,\phi) + V^{\{v_3\}}(\theta_2,\phi;R,\theta_1), \quad (2)$$

in which $\mu^{-1}=(2m_{\rm H})^{-1}+(2m_{\rm O}+m_{\rm C})^{-1}$, where $m_{\rm H}$, $m_{\rm C}$, and $m_{\rm O}$ are the masses of the H, C, and O atoms, respectively,[15] $B_{\rm CO_2}$ and $B_{\rm H_2}$ are the inertial rotational constant for CO_2 and H_2, respectively, and $V^{\{v_3\}}(\theta_2,\phi;R,\theta_1)$ is the effective vibrationally averaged intermolecular potential for H_2 interacting with CO_2 in vibrational state $(0,0,v_3)$. Also, $\hat{j}_1$ and $\hat{j}_2$ are the (vector) total angular momentum operators for CO_2 and H_2, respectively, and the overall total angular momentum operator is $\hat{J}=\hat{j}_1+\hat{j}_2+\hat{\ell}$, where $\hat{\ell}$ is the (vector) angular momentum operator for the rotation of the intermolecular axis $\vec{R}$.

The inertial rotational constant for *para*-H_2 (59.322 cm^{-1}) is more than 150 times larger than those of CO_2 in its ground (0.390 219 cm^{-1}) or (0,0,1) excited state (0.387 141 cm^{-1}).[16] It therefore seems reasonable to perform a Born–Oppenheimer-type separation of the fast rotational motion of *para*-H_2 from the slower motions associated with the other intermolecular degrees of freedom. A widely used version of this approach is to perform a simple-spherical average over the orientations of the H_2 moiety at each combination of R and θ_1, and then study the *para*-H_2-{molecule} dynamics on the resulting 2D (R,θ_1)-dependent PES. This has been done in studies of *para*-H_2 interacting with OCS,[6] with N_2O,[5] and with CO.[4] However, the accuracy of this approach may be expected to decrease rapidly with increasing strength of the intermolecular interaction.

A much better reduced-dimension description is obtained by applying what we call an adiabatic-hindered-rotor (AHR) approximation in which a *para*-H_2 located at any (R,θ_1) position relative to the CO_2 molecule is treated as a hindered-rotor subject to the two-dimensional angular potential $V^{\{v_3\}}(\theta_2,\phi;R,\theta_1)$, which is parametrically dependent on R and θ_1. In particular, for any particular (R,θ_1) configuration one can solve the 2D angular Schrödinger equation,

$$\hat{H}_{\rm H_2}(\theta_2,\phi;R,\theta_1)\Phi(\theta_2,\phi;R,\theta_1) = E_{\rm H_2}(R,\theta_1)\Phi(\theta_2,\phi;R,\theta_1), \quad (3)$$

and its lowest eigenvalues will define a 2D effective "hindered-rotor" PES,

$$V^{\rm 2D}_{\rm hind}(R,\theta_1) \equiv E_{\rm H_2}(R,\theta_1), \quad (4)$$

which governs the intermolecular dynamics defined by the resulting reduced-dimension Hamiltonian,

$$\hat{H}_{\rm rel}(R,\theta_1,\phi) = -\frac{\hbar^2}{2\mu}\frac{\partial^2}{\partial R^2} + B_{\rm CO_2}\hat{j}_1^2 + \frac{(\hat{J}-\hat{j}_1)^2}{2\mu R^2} + V^{2D}_{\rm hind}(R,\theta_1). \quad (5)$$

Equation (3) may be solved readily using a basis set of spherical harmonic functions,

$$\Phi(\theta_2,\phi;R,\theta_1) = \sum_L \sum_M c_{L,M}(R,\theta_1)Y_{L,M}(\theta_2,\phi). \quad (6)$$

However, if the expansion of Eq. (6) is collapsed to a single term,

$$\Phi(\theta_2,\phi;R,\theta_1) = \Phi(\theta_2,\phi) \approx Y_{L=0,\ M=0}(\theta_2,\phi), \quad (7)$$

the lowest eigenvalue of Eq. (3) effectively defines the simple spherically averaged 2D potential energy surface,

$$V^{\rm 2D}_{\rm spher}(R,\theta_1) = \int_0^{2\pi} d\phi \int_0^{\pi} d\theta_2 \sin\theta_2 V(\theta_2,\phi;R,\theta_1). \quad (8)$$

In the present work, 16-point Gaussian quadratures were used for integration over both θ_2 and ϕ, while the three even spherical harmonic functions corresponding to $L=0$, 2, and 4 were used to define $\Phi(\theta_2,\phi)$ for *para*-H_2 interactions, and the four even-order functions with $L=0$–6(2) were used for *ortho*-D_2. This sufficed to give convergence to better than 0.001 cm^{-1}.

III. RESULTS AND DISCUSSION

A. Angular-averaging and reduced-dimension potential energy surfaces

1. For *para*-H_2 and *ortho*-D_2 with CO_2

Figure 2 compares the reduced-dimension 2D potential energy surfaces for *para*-H_2 with ground-state $(v_3=0)CO_2$, which were obtained from the full 4D vibrationally averaged (over the Q_3 normal mode of CO_2) intermolecular potential of Ref. 17 using the adiabatic-hindered-rotor and "simple-spherical-average" approximations. The upper panel shows the spherical-average PES of Eq. (8) and the lower panel the hindered-rotor PES of Eq. (4). As is seen there and in Table I, both potentials have a global minimum located at a T-shaped geometry with $\theta_1=90°$, saddle points at near-linear

Downloaded 23 Sep 2010 to 129.97.80.64. Redistribution subject to AIP license or copyright; see http://jcp.aip.org/about/rights_and_permissions

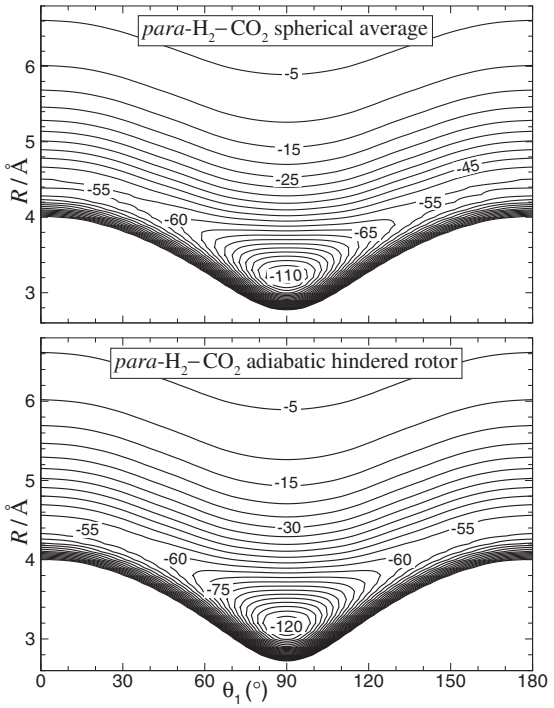

FIG. 2. Reduced-dimension spherical-average and adiabatic-hindered-rotor average 2D PESs for *para*-H_2–$CO_2(v_3=0)$.

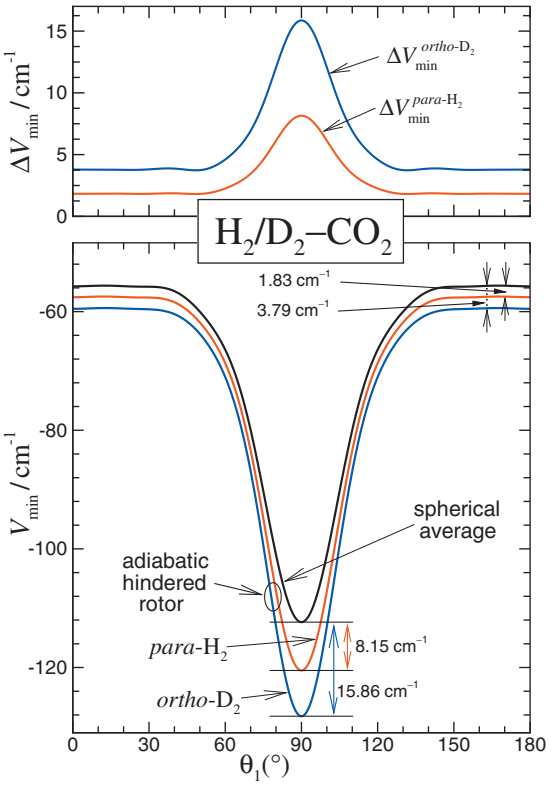

FIG. 3. Lower panel: minimum-energy paths on the reduced-dimension 2D spherical-average and hindered-rotor average potentials for *para*-H_2 or *ortho*-D_2 interacting with $CO_2(v_3=0)$. Upper panel: differences $[V_{spher}-V_{hinder}]$ along the minimum-energy paths in the lower panel.

geometries, and a very shallow second minimum at linear geometries where $\theta_1=0°$ or 180°. However, although their topographies are quite similar, the energies of the global minima on the two surfaces are quite different, and their radial locations are slightly different. In particular, the minimum of the hindered-rotor potential for *para*-H_2–CO_2 is 8.15 cm^{-1} deeper (by 7%) than that of the spherical-average potential, and that for *ortho*-D_2–CO_2 is 15.86 cm^{-1} deeper! However, the differences between the energies of the linear minima and transition states of the spherical-average and hindered-rotor potential are considerably smaller.

While the spherical-average potentials are identical for *para*-H_2- and *ortho*-D_2-{molecule} interactions, the corresponding hindered-rotor potentials are distinctly different because the fact that $B_{D_2}/B_{H_2}\approx 0.5$ means that solutions to Eq. (3) for *ortho*-D_2-{molecule} systems will have substantially larger contributions from basis functions corresponding to $L>0$. This is the reason for the factor of 2 increase in the differences of the energies at stationary points (see Table I). Similar differences are seen in the plots of the minimum-energy paths on the 2D spherical-average and adiabatic-hindered-rotor potentials shown in the lower panel of Fig. 3, and in the differences between the energies along these paths shown in its upper panel. The angular variation of these differences means that calculated level spacings on the hindered-rotor and spherical-average surfaces will be quite different. Details of our recommended analytic 2D hindered-rotor potentials for *para*-H_2– and *ortho*-D_2–$CO_2(v_3)$ are presented in the Appendix.

It is interesting to note that the binding energies of the

TABLE I. Properties of stationary points of the 2D reduced-dimension spherical-average and hindered-rotor-average potential energy surfaces for *para*-H_2–CO_2 and *ortho*-D_2–CO_2 for CO_2 in its ground ($v_3=0$, upper entry for each case) and excited ($v_3=1$, lower entries) states. The main entries are $\{R(Å), \theta_1^e, V_{min}(cm^{-1})\}$, and $\Delta V_{min}(cm^{-1})$ is the difference between the spherical-average and hindered-rotor energies.

		Para-H_2–CO_2		*Ortho*-D_2–CO_2	
	Spherical average	Hindered-rotor average	ΔV_{min}	Hindered-rotor average	ΔV_{min}
T-shaped minimum	{3.190, 90.0, −112.35}	{3.145, 90.0, −120.50}	8.15	{3.109, 90.0, −128.21}	15.86
	{3.191, 90.0, −112.48}	{3.147, 90.0, −120.54}	8.06	{3.111, 90.0, −128.19}	15.71
Saddle point	{4.404, 12.7, −55.62}	{4.398, 12.2, −57.46}	1.84	{4.385, 12.7, −59.40}	3.78
	{4.400, 13.6, −56.10}	{4.395, 13.0, −57.90}	1.80	{4.383, 13.5, −59.80}	3.70
Linear minimum	{4.438,180.0, −55.74}	{4.429,180.0, −57.57}	1.83	{4.420,180.0, −59.53}	3.79
	{4.439,180.0, −56.24}	{4.430,180.0, −58.03}	1.79	{4.421,180.0, −59.94}	3.70

Downloaded 23 Sep 2010 to 129.97.80.64. Redistribution subject to AIP license or copyright; see http://jcp.aip.org/about/rights_and_permissions

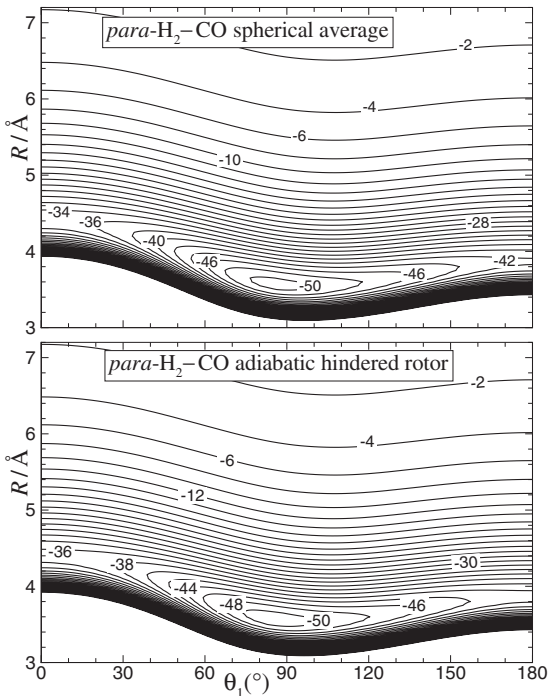

FIG. 4. Reduced-dimension spherical-average and adiabatic-hindered-rotor average 2D PESs for *para*-H_2−CO. The linear configuration *para*-H_2−C−O corresponds to $\theta_1=0°$.

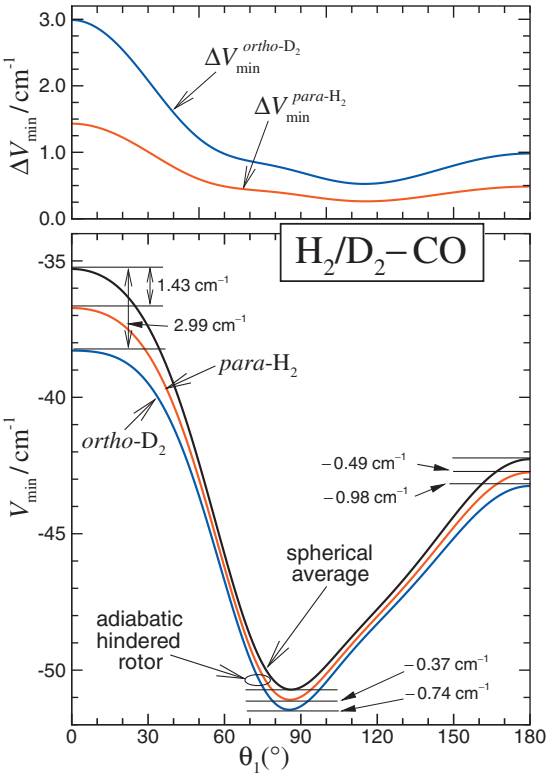

FIG. 5. Lower panel: minimum-energy paths on the reduced-dimension 2D spherical-average and hindered-rotor average potentials for *para*-H_2 or *ortho*-D_2 interacting with $CO_2(v_3=0)$. Upper panel: differences $[V_{spher}-V_{hinder}]$ along the minimum-energy paths in the lower panel.

various stationary points listed in Table I are almost a factor of 2 smaller than those for the corresponding points on the full 4D surface.[17] While the global minimum remains at a T-shaped configuration ($\theta_1=90°$), its radial position is somewhat larger here ($R_{min}=3.15$ versus 2.97 Å). Moreover, the 4D surface has no saddle point separating the global minimum and the collinear energy.

2. For *para*-H_2 and *ortho*-D_2 with CO

In general we expect that the difference between a simple-spherical average and an adiabatic-hindered-rotor treatment will decrease with the strength of the interaction. To examine this point, Figs. 4 and 5 repeat the comparisons of Figs. 2 and 3 for the case of *para*-H_2 with CO, for which the depth of the attractive well is less than half that for *para*-H_2−CO_2. These results are based on the vibrationally averaged (over H_2 stretching) 4D PES of Jankowski and Szalewicz.[18] Details of our 2D hindered-rotor potentials for this system are presented in the Appendix.

As was the case for *para*-H_2−CO_2, the adiabatic-hindered-rotor PES is everywhere deeper than that obtained using the "spherical-average" approximation, but the differences here are much smaller. In particular, although the overall interaction energy is roughly a factor of 2 weaker, the maximum value of the differences seen here is more than five times smaller. At the same time, the >1 cm^{-1} differences between the hindered-rotor and spherical-average 2D surfaces mean that dynamical simulation using these two approaches could yield somewhat different results.

As was also the case for the H_2/D_2−CO_2 system, these 2D *para*-H_2/*ortho*-D_2−CO surfaces are a factor of 2 shallower than is the full 4D PES from which they were determined.[18] However, in the present case the angular position of the global minimum changes from the collinear geometry with the H_2 at the carbon end of the molecule ($\theta_1=0°$) found for the 4D surface, to a near-perpendicular geometry ($\theta_1=85.8°$) for the hindered-rotor PES. Moreover, Fig. 5 shows that the configuration corresponding to the absolute minimum on the 4D surface turns out to be the *least-favored* minimum-energy arrangement on the reduced-dimension 2D surfaces. We also see that in this case the differences between the two angular-averaging approximations are relatively small at the 2D global minimum configuration, and largest at the least-favored (in the 2D picture) linear *para*-H_2−C−O alignment. Thus, other than the fact that the differences between the hindered-rotor and simple-spherical approaches decrease more rapidly than the interaction energies, few generalizations are evident.

3. For (*para*-H_2)$_2$ and (*ortho*-D_2)$_2$

The type of approximation being examined here will be most important for systems containing two or more *para*-H_2 or *ortho*-D_2 molecules, since dealing with all of the angular degrees of freedom would be very CPU-expensive. It is therefore desirable also to examine the importance of this type of approximation for pairs of *para*-H_2 or *ortho*-D_2 molecules. In this case we wish to separate off the rapid rotation of *both* hydrogen/deuterium molecules, so the wave function used for the angular motion is expanded as

Downloaded 23 Sep 2010 to 129.97.80.64. Redistribution subject to AIP license or copyright; see http://jcp.aip.org/about/rights_and_permissions

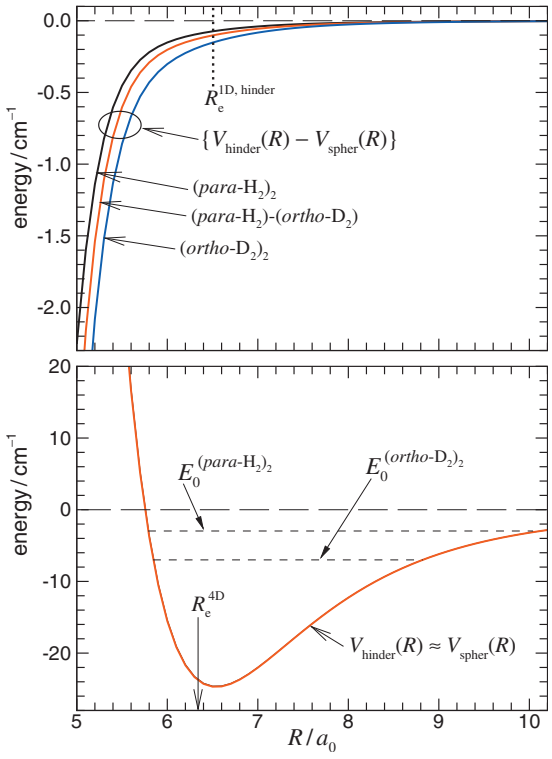

FIG. 6. Comparison of hindered-rotor and spherical-average 1D potentials for (*para*-H_2)$_2$ and (*ortho*-D_2)$_2$. R_e^{4D} indicates the position of the minimum on the full 4D H_2–H_2 PES (Ref. 19), and E_0 is the ground-state energy for the indicated species.

$$\Phi(\theta_1,\phi_1,\theta_2,\phi_2;R) = \sum_{L_1,M_1}\sum_{L_2,M_2} c_{L_1,M_1,L_2,M_2}(R) \times Y_{L_1,M_1}(\theta_1,\phi_1)Y_{L_2,M_2}(\theta_2,\phi_2). \quad (9)$$

Following this separation, the relative motion of the two *para*-H_2 molecules is governed by the simple one-dimensional (1D) Hamiltonian

$$\hat{H}_{rel}(R) = -\frac{\hbar^2}{2\mu}\frac{\partial^2}{\partial R^2} + \frac{\hat{\ell}^2}{2\mu R^2} + V^{1D}(R). \quad (10)$$

Using the vibrationally averaged 4D PES of Patkowski *et al.*,[19] Fig. 6 compares our hindered-rotor potentials for *para*-H_2 and *ortho*-D_2 with the simple-spherical average 1D potential, which is the same for both isotopologues. We see that the difference between these two potentials is very small at the equilibrium separation ($\Delta V^{1D}_{para\text{-}H_2}(R_e)=0.074$ cm^{-1}) or larger distances, although it grows sharply at smaller separations. However, although the resulting errors in the simple-spherical-average level energies are quite small (see below), they are still an order of magnitude larger those obtained using the hindered-rotor approximation. The properties of the recommended 1D hindered-rotor potentials obtained from the full 4D PES of Patkowski *et al.*[19] are presented in the Appendix.

As for the systems considered above, the well depth of our hindered-rotor pair potential is substantially smaller than that of the full 4D surface (24.71 versus 39.70 cm^{-1}), and the equilibrium distance slightly larger (6.54 versus 6.34 bohr).

B. Angular-averaging approximations and bound-state energies

An important test of the relative effectiveness of the angular-averaging methods described above is provided by comparisons of level energies on the full four-dimensional potential energy surfaces with those calculated from the associated 2D spherical-average and hindered-rotor-average surfaces. Table II presents such comparisons for the bimers formed by *para*-H_2 and *ortho*-D_2 with $CO_2(v_3)$, with CO, and with itself.

Quantum mechanical eigenvalue calculations on the full 4D potentials in Ref. 17 show that they support nine vibrational levels of *para*-H_2–$CO_2(v_3)$ for both $v_3=0$ and 1. In contrast, our 2D hindered-rotor potentials support eight bound states for both $v_3=0$ and 1, while the 2D spherical-average potential supports only seven bound states when CO_2 is in its ground state and eight when $v_3=1$. As is seen in Table II, the errors associated with the use of the spherical-average potentials are more than an order of magnitude larger than those obtained using the 2D hindered-rotor potentials. Moreover, the discrepancies for the spherical-average case are all positive, while those for the hindered-rotor model are all negative, except for the very highest level (see below). Note too that the band-origin shift calculated using the hindered-rotor potential, $\Delta\nu_0=-0.175$ cm^{-1} for *para*-H_2–CO_2, is in far better agreement with the -0.179 cm^{-1} shift implied by the full 4D surface than is the -0.217 cm^{-1} shift obtained using the 2D spherical-average PES. It is interesting to contrast the relatively close agreement seen here between the full 4D and 2D hindered-rotor binding energies, with the factor of 2 difference between the binding energies of the stationary points on the 4D and 2D surfaces.

The lower segments of Table II compare vibrational levels energies calculated using full 4D potentials for *para*-H_2–CO, *ortho*-D_2–CO, (*para*-H_2)$_2$, and (*ortho*-D_2)$_2$ with those generated using the reduced-dimension hindered-rotor and spherical-average potentials discussed above. Although all of these discrepancies are substantially smaller than those for the H_2/D_2–CO_2 systems, the errors in the hindered-rotor binding energies are still an order of magnitude smaller than those yielded by the spherical-average PESs.

It is interesting to note that all of the reduced-dimension potentials for *para*-H_2/*ortho*-D_2 with CO_2 and CO support fewer bound levels than do the corresponding full 4D potentials. This is qualitatively explained by the fact that the longest-range term contributing to the 4D potential is a quadrupole-quadrupole interaction which dies off as R^{-5}, while the process of taking a hindered-rotor or simple-spherical average of the H_2 orientations averages that term to zero, making the longest-range contribution to the 2D potentials the R^{-6} dispersion term. The growing relative importance of the R^{-5} term at large distances explains why the 4D potential supports more levels than do the approximate 2D surfaces.

Downloaded 23 Sep 2010 to 129.97.80.64. Redistribution subject to AIP license or copyright; see http://jcp.aip.org/about/rights_and_permissions

TABLE II. Comparison of energies (in cm^{-1}) of ($J=0$) vibrational levels calculated on the full 4D PES with those generated using reduced-dimension 2D (or 1D) potential energy surfaces obtained using the hindered-rotor and spherical-average approximations for *para*-H_2 and *ortho*-D_2 with CO_2, CO, and with itself. For the *para*-H_2/*ortho*-D_2–CO_2 systems, the first entry for each level is for the complex formed from ground-state $CO_2(v_3=0)$ and the second for the complex with $CO_2(v_3=1)$, while Δv_0 is the resulting band origin shift.

		differences{2D-4D}			differences{2D-4D}	
Level	4D	AHR	sph	4D	AHR	sph
		Para-H_2–CO_2			*Ortho*-D_2–CO_2	
1	−54.437	−0.404	4.303	−72.671	−0.822	9.731
	−54.616	−0.400	4.265	−72.802	−0.817	9.644
2	−31.013	−0.151	1.848	−46.306	−0.439	5.424
	−31.272	−0.150	1.836	−46.562	−0.437	5.385
3	−25.392	−0.078	1.260	−37.138	−0.266	3.852
	−25.660	−0.076	1.246	−37.391	−0.265	3.810
4	−22.006	−0.073	1.282	−32.929	−0.161	2.842
	−22.303	−0.071	1.267	−33.228	−0.157	2.805
5	−17.113	−0.096	1.519	−30.880	−0.175	3.478
	−17.405	−0.096	1.502	−31.175	−0.172	3.433
6	−9.046	−0.086	1.432	−24.970	−0.182	3.399
	−9.371	−0.085	1.418	−25.301	−0.181	3.361
7	−5.058	−0.091	1.207	−22.360	−0.219	4.376
	−5.242	−0.091	1.226	−22.625	−0.217	4.345
8	−0.756	0.044	⋯	−15.412	−0.183	3.096
	−0.912	0.037	0.850	−15.719	−0.184	3.092
9	−0.161	⋯	⋯	−11.774	−0.174	3.639
	−0.163	⋯	⋯	−12.135	−0.172	3.611
10	⋯	⋯	⋯	−6.840	−0.093	1.637
	⋯	⋯	⋯	−7.019	−0.092	1.655
11	⋯	⋯	⋯	−6.217	−0.052	1.266
	⋯	⋯	⋯	−6.373	−0.052	1.265
12	⋯	⋯	⋯	−4.051	−0.062	2.079
	⋯	⋯	⋯	−4.245	−0.061	2.068
13	⋯	⋯	⋯	−2.014	−0.058	1.153
	⋯	⋯	⋯	−2.203	−0.057	1.157
14	⋯	⋯	⋯	−0.347	−0.031	⋯
	⋯	⋯	⋯	−0.528	−0.043	⋯
15	⋯	⋯	⋯	−0.161	⋯	⋯
	⋯	⋯	⋯	−0.163	⋯	⋯
Δv_0	−0.179	0.004	−0.038	−0.131	0.005	−0.086
		para-H_2–CO			*ortho*-D_2–CO	
1	−19.528	−0.025	0.238	−25.840	−0.078	0.503
2	−12.354	−0.028	0.306	−18.742	−0.092	0.698
3	−4.275	−0.024	0.312	−11.702	−0.091	0.790
4	−0.117	⋯	⋯	−2.505	−0.018	0.225
5	⋯	⋯	⋯	−0.836	−0.041	0.409
6	⋯	⋯	⋯	−0.117	⋯	⋯
		(*para*-H_2)$_2$			(*ortho*-D_2)$_2$	
1	−2.966	−0.003	0.025	−6.995	−0.006	0.073

C. Angular-averaging approximations and infrared spectra of *para*-H_2–CO_2

Table III compares the energies of a representative set[20] of infrared transitions between ground intermolecular vibrational levels of *para*-H_2–$CO_2(v_3)$ for $v_3=0\rightarrow1$ calculated using the full 4D potential,[17] with those obtained using our reduced-dimension hindered-rotor and spherical-average 2D surfaces. In the upper half of the table all transition energies are expressed relative to the $v_3=1\leftarrow0$ band origin of CO_2, and in the lower half, they are expressed relative to the *para*-H_2–$CO_2(v_3)$ band origin.[20] On the "absolute" energy scale associated with the upper half of this table, we see that all spherical-average transition energies are distinctly too small, while those yielded by the hindered-rotor potentials are slightly too large. In contrast, for transition energies expressed relative to the band origin of the complex, the discrepancies for both cases can be either positive or negative.

Downloaded 23 Sep 2010 to 129.97.80.64. Redistribution subject to AIP license or copyright; see http://jcp.aip.org/about/rights_and_permissions

TABLE III. Comparisons of some infrared transition energies calculated from the 2D hindered-rotor and spherical-average potential energy surfaces with those generated from the full 4D potential energy surfaces for $H_2-CO_2(v_3)$. All energies are in cm^{-1}, and $\Delta\nu(2D-4D) \equiv \nu_{calc}(2D) - \nu_{calc}(4D)$.

		2D MLR			
Transitions	4D MLR	Hindered-rotor		Spherical average	
$J'_{K'_aK'_c} - J''_{K''_aK''_c}$	$\nu_{calc}(4D)$	$\nu_{calc}(2D)$	$\Delta\nu(2D-4D)$	$\nu_{calc}(2D)$	$\Delta\nu(2D-4D)$
Relative to the 2349.1433 cm^{-1} band origin of CO_2					
$1_{01}-0_{00}$	0.472	0.476	0.004	0.434	−0.038
$1_{10}-1_{11}$	−0.030	−0.027	0.003	−0.063	−0.033
$2_{12}-1_{11}$	0.968	0.972	0.004	0.924	−0.044
$1_{01}-2_{02}$	−1.457	−1.454	0.003	−1.489	−0.032
$2_{21}-2_{02}$	1.554	1.565	0.011	1.446	−0.108
$2_{21}-2_{20}$	−0.225	−0.221	0.004	−0.265	−0.040
$3_{03}-2_{02}$	1.623	1.628	0.005	1.570	−0.053
$3_{21}-2_{02}$	3.663	3.673	0.010	3.563	−0.100
$3_{21}-2_{20}$	1.884	1.888	0.004	1.852	−0.032
$1_{10}-2_{11}$	−1.644	−1.641	0.003	−1.683	−0.039
$2_{12}-2_{11}$	−0.646	−0.641	0.005	−0.697	−0.051
$3_{12}-2_{11}$	1.955	1.959	0.004	1.918	−0.037
$2_{12}-3_{13}$	−1.902	−1.900	0.002	−1.927	−0.025
$4_{14}-3_{13}$	2.041	2.047	0.006	1.986	−0.055
Average			0.005_1		−0.049
RMSD			0.005_1		0.054
Relative to the 2348.9452 cm^{-1} band origin of *para*-H_2-CO_2					
$1_{01}-0_{00}$	0.652	0.652	0.000	0.651	−0.001
$1_{10}-1_{11}$	0.149	0.148	−0.001	0.154	0.005
$2_{12}-1_{11}$	1.147	1.148	0.001	1.140	−0.007
$1_{01}-2_{02}$	−1.278	−1.279	−0.001	−1.272	0.006
$2_{21}-2_{02}$	1.733	1.740	0.007	1.663	−0.070
$2_{21}-2_{20}$	−0.045	−0.045	0.000	−0.048	−0.003
$3_{03}-2_{02}$	1.802	1.804	0.002	1.787	−0.015
$3_{21}-2_{02}$	3.843	3.849	0.006	3.780	−0.063
$3_{21}-2_{20}$	2.064	2.064	0.000	2.069	0.005
$1_{10}-2_{11}$	−1.465	−1.465	0.000	−1.466	−0.001
$2_{12}-2_{11}$	−0.467	−0.466	0.001	−0.480	−0.013
$3_{12}-2_{11}$	2.134	2.134	0.000	2.134	0.000
$2_{12}-3_{13}$	−1.723	−1.724	−0.001	−1.710	0.013
$4_{14}-3_{13}$	2.221	2.222	0.001	2.203	−0.018
Average			0.001_4		-0.012_2
RMSD			0.003_7		0.026_7

However, in either case, the average and root mean square deviations (RMSD) of the predictions yielded by the hindered-rotor reduced-dimension surface are an order of magnitude smaller for than those generated from the spherical-average 2D surface.

In summary, we see that even when dealing with transitions between pure rotational levels on the upper and lower surfaces, a very substantial improvement in accuracy is obtained if the hindered-rotor model is used rather than the conventional simple-spherical-average approach. The results in Table II then show that the errors associated with the latter will be orders of magnitude larger if the transitions also involve intermolecular vibrational excitation. Thus, even though predicted spectroscopic transition energies involves differences between level energies on the upper and lower surfaces, the advantages of using the hindered-rotor reduced-dimension model remain very substantial.

IV. CONCLUSIONS

This paper critically compares two methods for averaging over H_2 orientations to obtain reduced-dimension potential energy surfaces for *para*-H_2/*ortho*-D_2-{molecule} systems. It shows that there are substantial differences between the effective potentials yielded by these two approximations, and that the magnitude of these difference increase sharply with the strength of the interaction and complexity of the molecular partner. Moreover, comparison of either binding energies or spectroscopic transition energies shows that the hindered-rotor model yields results quite close to those obtained from the full 4D surface, while predictions generated using the simple-spherical average approximation are at least an order of magnitude worse. The computational effort required to generate reduced-dimension hindered-rotor potentials is relatively modest so it seems clear that this approach should be strongly preferred whenever one wishes to use a

Downloaded 23 Sep 2010 to 129.97.80.64. Redistribution subject to AIP license or copyright; see http://jcp.aip.org/about/rights_and_permissions

reduced-dimension approach to simulate dynamical properties of systems including *para*-H_2 or *ortho*-D_2 molecules. It is important to remember, however, that different effective potentials are required for interactions of a given molecule with *para*-H_2 and *ortho*-D_2.

APPENDIX: ANALYTIC REDUCED-DIMENSION POTENTIALS FOR *PARA*-H_2 AND *ORTHO*-D_2 INTERACTING WITH CO_2, WITH CO, AND WITH THEMSELVES

The 1D effective radial potential obtained for *para*-H_2 or *ortho*-D_2 interacting with itself may be represented using the Morse/long-range (MLR) radial potential energy function of Ref. 21. This potential has the form

$$V_{\mathrm{MLR}}(R) = \mathfrak{D}_e\left(1 - \frac{u_{\mathrm{LR}}(R)}{u_{\mathrm{LR}}(R_e)} e^{-\beta(R)\cdot y_p^{\mathrm{eq}}(R)}\right)^2, \tag{A1}$$

in which $\mathfrak{D}_e$ is the well depth and $u_{\mathrm{LR}}(R)$ defines the attractive limiting long-range behavior. Since *para*-H_2 or *ortho*-D_2 is being treated as a spherical particle, the leading contribution to this long-range behavior is the dispersion energy, for which we use the three-term expression

$$u_{\mathrm{LR}}(R) = \frac{C_6}{R^6} + \frac{C_8}{R^8} + \frac{C_{10}}{R^{10}}. \tag{A2}$$

The radial distance variable in the exponent of Eq. (A1) is the dimensionless quantity

$$y_p^{\mathrm{eq}}(R) = \frac{R^p - {R_e}^p}{R^p + {R_e}^p}, \tag{A3}$$

in which R_e is the position of the potential minimum and p is a small positive integer which must be larger than the difference between the largest and smallest of the (inverse) powers appearing in the definition of $u_{\mathrm{LR}}(R)$, so here $p=5$.[22] The exponent coefficient in Eq. (A1) is a relatively slowly varying function which is written as the constrained polynomial[21]

$$\beta(R) = \beta_\infty y_p^{\mathrm{ref}}(R) + [1 - y_p^{\mathrm{ref}}(R)]\sum_{i=0}^{N} \beta_i y_q^{\mathrm{ref}}(r)^i, \tag{A4}$$

whose behavior is expressed in terms of the two radial variables,

$$y_p^{\mathrm{ref}}(R) = \frac{R^p - {R_{\mathrm{ref}}}^p}{R^p + {R_{\mathrm{ref}}}^p} \quad \text{and} \quad y_q^{\mathrm{ref}}(R) = \frac{R^q - {R_{\mathrm{ref}}}^q}{R^q + {R_{\mathrm{ref}}}^q}, \tag{A5}$$

in which R_{ref} is a reference distance which is usually set $\geq R_e$, and the integer q is usually set in the range $1 < q \leq p$.[21] The definition $\beta_\infty \equiv \ln\{2\mathfrak{D}_e/u_{\mathrm{LR}}(r_e)\}$ means that an MLR potential will have the limiting long-range behavior defined by the selected definition of $u_{\mathrm{LR}}(r)$. In the present treatment of (*para*-H_2)$_2$, we set $q=2$ and fixed $R_{\mathrm{ref}}=R_e$.

For a dense mesh of R values on the range of 3–30 bohr, a hindered-rotor treatment using the wave function expansion of Eq. (9) was applied to the analytic 4D PES of Patkowski *et al.*[19] for each of the species (*para*-H_2)$_2$, (*para*-H_2)(*ortho*-D_2), and (*ortho*-D_2)$_2$. Potential energy values below 1000 cm^{-1} above the dissociation asymptote were then fitted to 1D MLR potentials using the $u_{\mathrm{LR}}(R)$ long-range potential of Eq. (A2) with the spherically averaged C_6, C_8, and C_{10} coefficients from Refs. 19, 23, and 24. In these fits, potential functions values in the well and up to a repulsive wall energy of $+\mathfrak{D}_e$ are weighted equally, while higher repulsive wall energies are assigned weights which were reduced by the factor $[\mathfrak{D}_e/V(R)]^2$. Fits corresponding to rms discrepancies of ~0.000 35 cm^{-1} in the well region were obtained with $\{p,q\}=\{5,2\}$, $R_{\mathrm{ref}}=R_e$, and seven β_i exponent expansion coefficients. The full list of potential function parameters for this case is part of the supplementary data file submitted with the manuscript.[25]

Our reduced-dimension 2D *para*-H_2/*ortho*-D_2-{linear molecule} potentials are expressed using the generalized version of this MLR radial potential form described in Ref. 17. In particular, each of the parameters $\mathfrak{D}_e$, R_e, C_n, and β_i is written as a Legendre expansion,[26]

$$F(\theta_1) = \sum_{\lambda=0} F_\lambda P_\lambda(\cos\,\theta_1), \tag{A6}$$

in which $F=\mathfrak{D}_e$, R_e, C_n, or β_i. In addition, in order to allow the expansion center in the radial variables of Eq. (A5) to vary with θ_1, the additional parameter f_{ref} is introduced where $R_{\mathrm{ref}}(\theta_1)=f_{\mathrm{ref}}R_e(\theta_1)$. For the *para*-$H_2$/*ortho*-$D_2$–$CO_2$ system, the long-range potential was defined in terms of the two leading dispersion coefficients, $C_6(\theta)$ and $C_8(\theta)$, and the symmetry of the molecule means that only even values of λ contribute to Eq. (A6). In contrast, for *para*-H_2 and *ortho*-D_2–CO, terms corresponding to both even and odd values of λ contribute, and $u_{\mathrm{LR}}(R,\theta)$ also has a quadrupole/induced-dipole $C_7(\theta)/R^7$ term.

Starting from the vibrationally averaged 4D H_2/D_2–$CO_2(v_3)$ potential energy surfaces in Ref. 17, reduced-dimension 2D potentials for $v_3=0$ and 1 were obtained by performing 2D hindered-rotor calculations at all (R,θ_1) configurations for which *ab initio* points had been generated. The resulting potential function values at energies below 1000 cm^{-1} were fitted to the 2D MLR form with $p=q=3$, $f_{\mathrm{ref}}=1.0$, and an exponent polynomial order of $N=5$.

Similarly, starting from the analytic, vibrationally averaged (over the H_2 stretching coordinate) 4D potential energy surface of Jankowski and Szalewicz[18] reduced-dimension 2D potentials for *para*-H_2/*ortho*-D_2–$CO(v=0)$ were obtained by performing 2D hindered-rotor calculations on a dense mesh of (R,θ_1) values (θ_1 varying from 0° to 180° in steps of 5°, and 37 R values ranging from 2 to 12 Å). The resulting potential function values at energies below 500 cm^{-1} were then fitted to a 2D MLR form with $p=q=3$, $f_{\mathrm{ref}}=1.6$, and an exponent polynomial order of $N=4$. For all of these cases, the associated sets of F_λ parameters are listed in the supplementary data file submitted with the manuscript.[25]

[1] Y. Kwon and K. B. Whaley, Phys. Rev. Lett. **89**, 273401 (2002).
[2] C. Piccarreta and F. A. Gianturco, Eur. Phys. J. D **37**, 93 (2006).
[3] F. Paesani and K. B. Whaley, J. Chem. Phys. **124**, 234310 (2006).
[4] S. Moroni, M. Botti, S. De Palo, and A. R. W. McKellar, J. Chem. Phys. **122**, 094314 (2005).
[5] H. Zhu and D. Xie, J. Comput. Chem. **30**, 841 (2009).
[6] F. Paesani and K. B. Whaley, Mol. Phys. **104**, 61 (2006).
[7] R. J. Le Roy and J. van Kranendonk, J. Chem. Phys. **61**, 4750 (1974).
[8] S. L. Holmgren, M. Waldman, and W. Klemperer, J. Chem. Phys. **67**,

Downloaded 23 Sep 2010 to 129.97.80.64. Redistribution subject to AIP license or copyright; see http://jcp.aip.org/about/rights_and_permissions

4414 (1977).
[9] M. H. Alexander, S. Gregurick, P. J. Dagdigian, G. W. Lemire, M. J. McQuaid, and R. C. Sausa, J. Chem. Phys. **101**, 4547 (1994).
[10] M. H. Alexander and M. Yang, J. Chem. Phys. **103**, 7956 (1995).
[11] M. H. Alexander, J. Chem. Phys. **108**, 4467 (1998).
[12] A. van der Avoird, P. E. S. Wormer, and R. Moszynski, Chem. Rev. (Washington, D.C.) **94**, 1931 (1994).
[13] J. Z. H. Zhang, J. Dai, and W. Zhu, J. Phys. Chem. A **101**, 2746 (1997).
[14] S. Y. Lin and H. Guo, J. Chem. Phys. **117**, 5183 (2002).
[15] G. Audi, A. H. Wapstra, and C. Thibault, Nucl. Phys. A **729**, 337 (2003).
[16] G. Guelachvili, J. Mol. Spectrosc. **79**, 72 (1980).
[17] H. Li, P.-N. Roy, and R. J. Le Roy, J. Chem. Phys. **132**, 214309 (2010).
[18] P. Jankowski and K. Szalewicz, J. Chem. Phys. **123**, 104301 (2005).
[19] K. Patkowski, W. Cencek, P. Jankowski, K. Szalewicz, J. B. Mehl, G. Garberoglio, and A. H. Harvey, J. Chem. Phys. **129**, 094304 (2008).
[20] A. R. W. McKellar, J. Chem. Phys. **122**, 174313 (2005).
[21] R. J. Le Roy, N. Dattani, J. A. Coxon, A. J. Ross, P. Crozet, and C. Linton, J. Chem. Phys. **131**, 204309 (2009).
[22] R. J. Le Roy and R. D. E. Henderson, Mol. Phys. **105**, 663 (2007).
[23] D. M. Bishop and J. Pipin, Int. J. Quantum Chem. **45**, 349 (1993).
[24] D. Spelsberg, T. Lorenz, and W. Meyer, J. Chem. Phys. **99**, 7845 (1993).
[25] See supplementary material at http://dx.doi.org/10.1063/1.3476465 for ASCII files listing the MLR expansion parameters defining the 1D adiabatic-hindered-rotor MLR potentials for $(para\text{-}H_2)_2$ and $(ortho\text{-}D_2)_2$ and the 2D AHR potentials for $para$-H_2 and $ortho$-D_2 interacting with CO and with $CO_2(v_3)$ for $v_3=0$ and 1, together with FORTRAN subroutines for generating the 2D surfaces.
[26] H. Li and R. J. Le Roy, Phys. Chem. Chem. Phys. **10**, 4128 (2008).

Downloaded 23 Sep 2010 to 129.97.80.64. Redistribution subject to AIP license or copyright; see http://jcp.aip.org/about/rights_and_permissions